Optics & Laser Technology 136 (2021) 106728

Contents lists available at ScienceDirect

Optics and Laser Technology

journal homepage: www.elsevier.com/locate/optlastec

Full length article

A mean shift segmentation morphological filter for airborne LiDAR DTM extraction under forest canopy

Zhenyang Hui [a,b,c], Shuanggen Jin [b,d], Yuanping Xia [a,*], Yunju Nie [a], Xiaowei Xie [a], Na Li [a]

[a] Faculty of Geomatics, East China University of Technology, Nanchang 330013, China
[b] School of Remote Sensing and Geomatics Engineering, Nanjing University of Information Science and Technology, Nanjing 210044, China
[c] Nanjing Longyuan Microelectronic Technology Co., Ltd, Nanjing 211106, China
[d] Shanghai Astronomical Observatory, Chinese Academy of Sciences, Shanghai 200030, China

ARTICLE INFO

Keywords:
Airborne LiDAR
Filtering
Mean shift
Morphological filter
Forested environment

ABSTRACT

In recent years, many airborne point clouds filtering methods have been developed. However, it is still challenging for distinguishing ground and non-ground points in forested areas due to the rugged terrains, dense vegetation canopy and low-level penetration of laser pulses. To derive satisfactory filtering results, this paper proposed a mean shift segmentation morphological filter. In this method, the mean shift segmentation is used for acquiring object primitives to determine filtering window sizes automatically. The point clouds detrending is proposed for improving the adaptability towards sloped terrains. A point cloud shifting in x and y directions technique is developed to acquire more ground seeds for generating a more accurate trending surface. Finally, the filtered ground points by the progressive morphological filter are recovered by adopting the surface-based filtering strategy. The proposed method is tested and validated using 14 samples with different forested environments. Experimental results show that the proposed method can achieve the average total error of 1.11%. The kappa coefficients of all these 14 samples are larger than 90% and the average kappa coefficient is 96.43%. The average root mean square error (RMSE) of the proposed method is 0.63. All these indicators are the best when compared to some other famous filtering methods.

1. Introduction

Airborne light detection and ranging (LiDAR) is an advanced automatic high precision stereo scanning technology [1], which is an important technological revolution in surveying and mapping after global positioning system (GPS). Compared to traditional measurement techniques, LiDAR can obtain high-density point clouds with three-dimensional (3-D) coordinates in non-contact active means [2,3]. When acquiring field data, airborne LiDAR is less affected by external environments. Moreover, laser pulses can penetrate forest canopy to get topographic information [4,5]. Thus, airborne LiDAR has been widely used in forest inventory and management, such as forest vegetation parameters retrieval, above ground biomass estimation and carbon cycle analysis [6–10].

To realize all these above-mentioned forestry applications, one fundamental step is the filtering. Filtering is the process of separating ground points from non-ground points [11]. In the past two decades, many famous filtering methods have been proposed, which can be classified into four categories, including slope, morphology, surface and segmentation based approaches [12–14].

In the slope-based methods, terrain is assumed as a continuous surface. The points with larger slopes are determined as non-ground points [15]. Susaki (2012) improved this kind of method to make the slope-based methods be adaptive to abrupt terrains [16]. Generally speaking, the slope-based approaches perform well in flat terrains. However, when encountering sloped topography, the filtering results of this kind of methods are sensitive to the slope threshold settings [17]. The classical morphological filter was originally proposed by Kilian et al. (1996). In their method, morphological opening operation is involved [18]. Zhang et al. (2003) further improved this method, where the morphological windows are changed gradually to filter objects with different sizes [19]. However, this kind of methods is easy to flatten terrain details [20–24]. Moreover, the maximum morphological window that is crucial for filtering performance generally needs to be set

* Corresponding author.
E-mail addresses: huizhenyang2008@ecut.edu.cn (Z. Hui), sgjin@shao.ac.cn (S. Jin), ypxia@ecut.edu.cn (Y. Xia), yjnie@ecut.edu.cn (Y. Nie), xwxie@ecut.edu.cn (X. Xie), 18846133671@163.com (N. Li).

https://doi.org/10.1016/j.optlastec.2020.106728
Received 7 May 2020; Received in revised form 28 August 2020; Accepted 31 October 2020
Available online 29 November 2020
0030-3992/

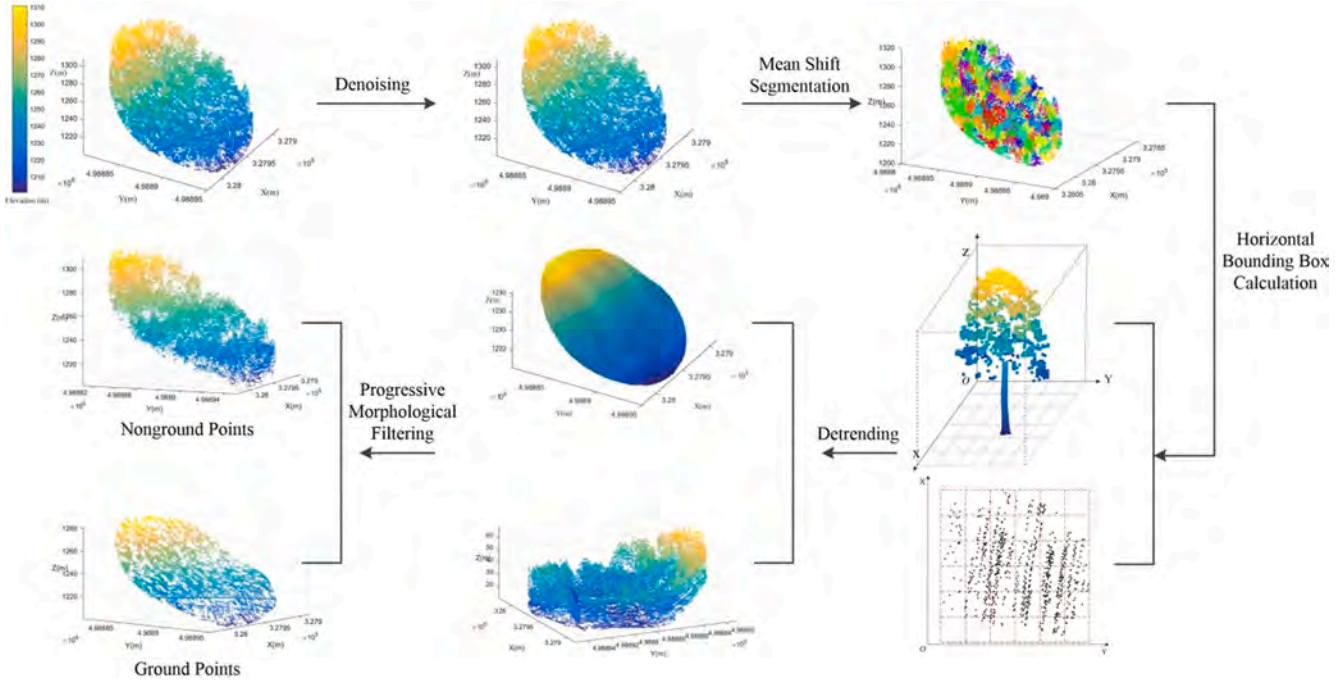

Fig. 1. Flowchart of the proposed method.

manually [5,25]. The surface-based methods realize filtering with the help of a rough interpolated surface. The rough surface can be generated using interpolators, such as thin plate spline (TPS) [26–29]. By calculating residuals between points and the interpolated surface, filtering results can be achieved. The rough surface can also be built using triangular irregular network (TIN) [30–32]. Axelsson (2000) proposed a classical progressive TIN densification (PTD) filtering method. This method has been tested by Sithole and Vosselman (2004) to own the best performance [33]. However, the PTD method has difficulties in processing abrupt terrains and terrains with attached objects. To solve this problem, Cai et al. (2019) improved the PTD method by combing with another famous filtering method called as CSF (Cloth Simulation Filter) that is developed by Zhang et al. (2016) [34,35]. The segmentation-based methods can be seen as object-based filters. Point clouds are first segmented into several individual units before filtering. Then some traditional filtering methods can be adopted to filter these units instead of single points [17,36,37]. Obviously, this kind of methods can achieve greater efficiency. However, the filtering performances rely heavily on the segmentation results.

Generally speaking, most filtering algorithms perform well in flat and simple sceneries [38–40]. However, when encountering steep landscapes with dense vegetation most filters present problems. On the one hand, there are less laser pulses that can reach the ground under the dense forest canopy. Less point clouds are hard to produce high precision filtering results. On the other hand, most filters assume that the bare-earth surface is smooth and continuous [13]. Thus, some rugged forest terrains are easily misclassified as non-ground points. To obtain better filtering results in forested areas, some specific filters were developed for DTM extraction under forest canopy. Kraus and Pfeifer (1998) presented a forest filtering method based on linear prediction, which is one of the category of surface-based filters mentioned above [41]. In their method, a rough surface is built iteratively by means of a weighted linear least-square interpolator. In each iteration, the elevation differences between the points and the rough surface are acquired. The points with negative elevation differences are set to high weights when generating the surface since these points are more likely ground points. Meanwhile, the points with positive residuals are assigned to low weights. The ground surface can be acquired keeping iterating the process mentioned above. Evans and Hudak (2007) proposed a multiscale curvature classification (MCC) method for filtering in vegetation environments [42]. This method is also a surface-based filter. The surface is built by TPS interpolation. The non-ground points are filtered iteratively if their elevations exceed the curvature of the surface. In the method proposed by Vega et al. (2012) four steps are involved, including lowest points extraction, distinct object points removal, lower object points removal and ground points densification [43]. Maguya et al. (2013) developed an iterative method for obtaining digital terrain model (DTM) from point clouds in steep forested terrain [44]. In their method, point clouds are first portioned and then a section of the DTM is estimated with the help of a fitted surface. Experiments indicate that this method performs well in the steep terrains with low LiDAR point densities. Zhao et al. (2016) improved the traditional PTD method to cope with different forested terrains. The main advantage of this method is that more accurate initial ground seeds can be acquired using the morphological method [45]. Lim and Liu (2018) developed a novel morphological filter using voxels. Point clouds are first voxelized and then non-ground points are removed step by step using several constraints [46]. Bigdeli et al. (2018) put forward a filtering approach for DTM extraction in the forest environment [47]. To make the interpolated surface more accurate, a modified invasive weed optimization method is developed. Montealegre et al. (2015) and Zhao et al. (2018) have compared several famous filtering methods in vegetation environments [48,49]. Montealegre et al. (2015) find that MCC method performs the best in the forest environment, which is in agreement with the conclusion made by Zhao et al. (2018). To improve the filtering performance in the rugged terrains with dense vegetation, Chen et al. (2020) developed a multi-level interpolation-based filter. In their method, more ground seeds can be acquired by adopting multi-scale morphological operations and robust z-score. Moreover, the residual threshold can be adaptive to different terrain environments [50].

However, all above mentioned methods are still challenging for accurately distinguishing ground and object points in forested areas due to the rugged terrains, dense vegetation canopy and low-level penetration of laser pulses. This paper proposed a novel improved morphological filter for DTM extraction under forest canopy. The proposed method is expected to have strong robustness to different forested environments.

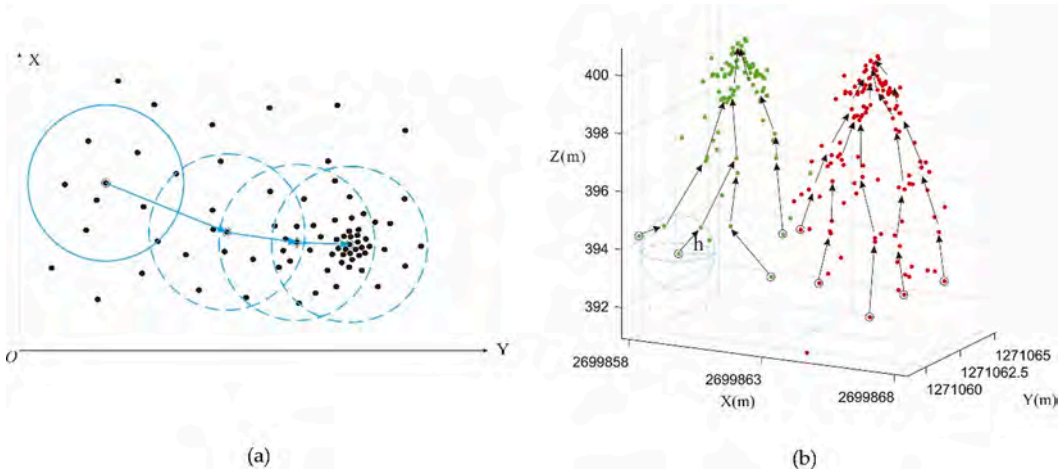

Fig. 2. Mean shift clustering process for 2-D and 3-D points: (a) 2-D points; (b) 3-D points. h is the bandwidth.

Moreover, this method can remove non-ground points effectively while protecting terrain details. Compared with other filtering methods, this paper owns the following three main contributions:

i Mean shift segmentation is used to determine the morphological filtering windows automatically, which enhances the robustness and automation for unknown environments.

ii Point cloud detrending is proposed in this paper, which assures the adaptability of the filter achieving good filtering performance in forested areas with sloped terrains.

iii A surface-based ground points retrieval scheme is combined with the progressive morphological filter, which can recover the filtered points on the protruding terrains as ground points, thereby protecting terrain details.

In the following, Section 2 describes the principle of the proposed method. In Section 3, experiments are designed to test the performance of the proposed method. Results are presented and compared with some other famous filtering algorithms in Section 4, and finally, Section 5 summarizes main conclusions.

2. Methodology

The flowchart of the proposed method is shown in Fig. 1. In general, the obtained point clouds always contain high and low outliers. These outliers, especially low outliers should be first removed since the points with lowest elevations are always assumed as ground points. This paper eliminates these low outliers using the morphological black top-hat (BTH) transformation presented by Li et al. (2017) [5]. The points with larger BTH results and fewer neighbors are low outliers. To determine the optimal maximum morphological filtering window automatically, this paper first obtains object primitives using mean shift segmentation. Then horizontal bounding box is calculated for each object primitive. The morphological filtering windows are set as the serials of sizes of horizontal bounding boxes. The benefits for doing this are twofold. On the one hand, the optimal maximum window size can be acquired. On the other hand, the number of morphological filtering iterations can be reduced to improve implementation efficiency. To make the filtering method adaptive to complex forested environments, point clouds detrending is proposed by subtracting a trending surface generated using radial basis function (RBF) interpolator with ground seeds. To acquire more ground seeds for generating an accurate trending surface, a point cloud shifting in x and y directions technique is developed. Finally, a surface-based ground points retrieval scheme is combined with the progressive morphological filter, which can recover the filtered points on the protruding terrains as ground points, thereby protecting terrain details. The proposed method mainly consists of the following four steps, including i Object primitive acquisition by mean shift segmentation, ii Horizontal bounding box calculation, iii Point cloud detrending, and iv Progressive morphological filtering.

2.1. Object primitive acquisition by mean shift segmentation

Mean shift is originally used for two-dimensional (2-D) image segmentation. It can realize image segmentation by constantly searching the local maximum of probability density function. In so doing, each point will converge to the mode through repeated iteration [51]. Points with the same or similar modes will be aggregated into the same class. By extending the 2-D kernel function to the 3-D kernel function, the mean shift method can be applied to point cloud segmentation [52]. Fig. 2 (a) and (b) illustrate the mean shift clustering process for 2-D and 3-D points, respectively.

In the mean shift method, mean shift vector $Ms(v_i)$ should be calculated first, which is defined as Eq. (1):

$$Ms(v_i) = \frac{\sum_{j=1}^{n} v_j g\left(\left\|\frac{v_i - v_j}{h}\right\|^2\right)}{\sum_{j=1}^{n} g\left(\left\|\frac{v_i - v_j}{h}\right\|^2\right)} - v_i \tag{1}$$

where $v_i = (x_i, y_i, z_i)$, n is the number of all the points. $g(\cdot)$ is the kernel function, which is defined as Eq. (2). h is the bandwidth, which is the only parameter involved in the mean shift segmentation. The bandwidth has an influence on the segmentation results. In general, the bandwidth should be set according to the specific tree crown sizes in the forest environments [53]. In this study, the mean shift method is used to segment object primitive for calculating the filtering window sizes. Individual tree does not need to be segmented very correctly. Thus, the bandwidth can be set as a constant roughly only if its value is a little larger than the crown sizes in the testing area. To make the mean shift segmentation easy to implement, this study set the bandwidth h as a constant, which is equal to 5 m in this paper.

$$g\left(\left\|\frac{v_i - v_j}{h}\right\|^2\right) = \begin{cases} exp\left(-\frac{1}{2}\left\|\frac{v_i - v_j}{h}\right\|^2\right), & if \left\|\frac{v_i - v_j}{h}\right\| <= 1 \\ 0, & otherwise \end{cases} \tag{2}$$

As shown in Fig. 2, the mean shift vector always points in the direction where the probability density goes up. This process will be converged into a mode after several iterations. This procedure can be represented by Eq. (3).

$$v_i^{t+1} \leftarrow v_i^t + Ms\left(v_i^t\right) \tag{3}$$

When the variation of $Ms\left(v_i^t\right)$ in the last two iterations is less than a threshold, it indicates that the mean shift vector has converged to the

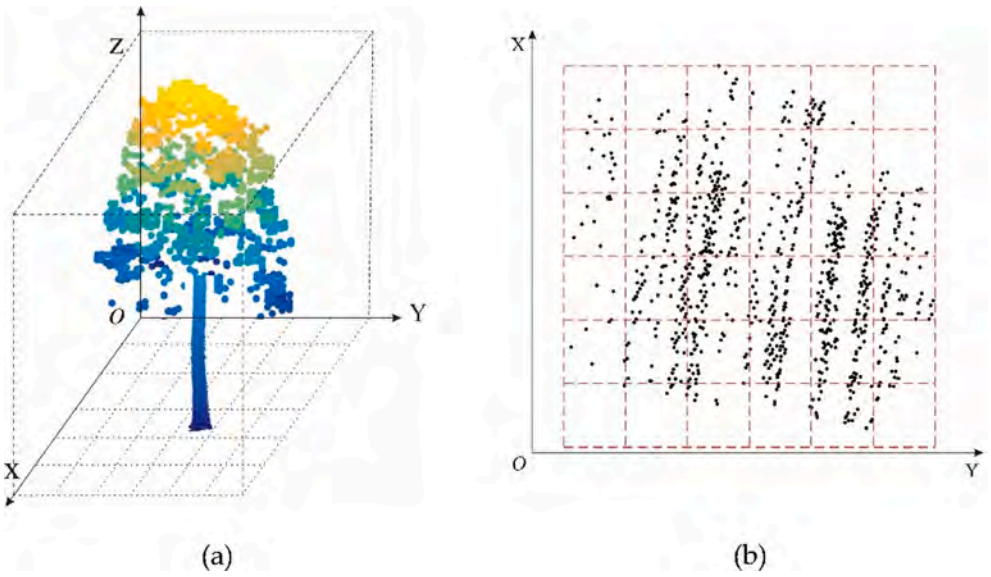

Fig. 3. Horizontal bounding box calculation: (a) Bounding box of a single 3-D tree; (b) Horizontal bounding box.

mode. Points with the same or similar modes will be assigned the same category labels, thereby achieving object primitives.

2.2. Horizontal bounding box calculation

To most morphology-based filtering methods, filtering windows affect the filtering performance directly. Generally, window sizes need to be set empirically by experienced staffs. However, it will still be difficult when encountering different terrain environments [5]. In this paper, the filtering window sizes are determined automatically based on the horizontal bounding box calculation towards object primitives that obtained by the mean shift segmentation. In so doing, there will be no need to define window sizes. For forested environment, the dominant objects are vegetation. Thus, the obtained object primitives using mean shift method are mainly trees. However, some parts of bare-earth can also form object primitives. In the morphological filtering method, the window size should be larger than the largest object in the tested areas. In other words, the maximum filtering window for forested areas should be larger than the largest size of tree canopy. Therefore, bare-earth primitives should be first separated from tree primitives. Considering the fact that the elevations of points in the tree primitives generally vary greatly, bare-earth primitives can be detected according to the standard deviation of elevations of each primitive, which is defined as Eq. (4).

$$std\left(Obj^i\right) = \sqrt{\frac{\sum_{j=1}^{k}\left(Obj^i.z_j - Obj^i.\bar{z}\right)^2}{k}} \tag{4}$$

where Obj^i is the i-th object primitive, $std(\cdot)$ is its corresponding standard deviation. $Obj^i.z_j$ is the z coordinate of j-th point in the object primitive, while $Obj^i.\bar{z}$ is the mean z coordinate of the i-th object primitive. The primitives with smaller standard deviations will be detected as bare-

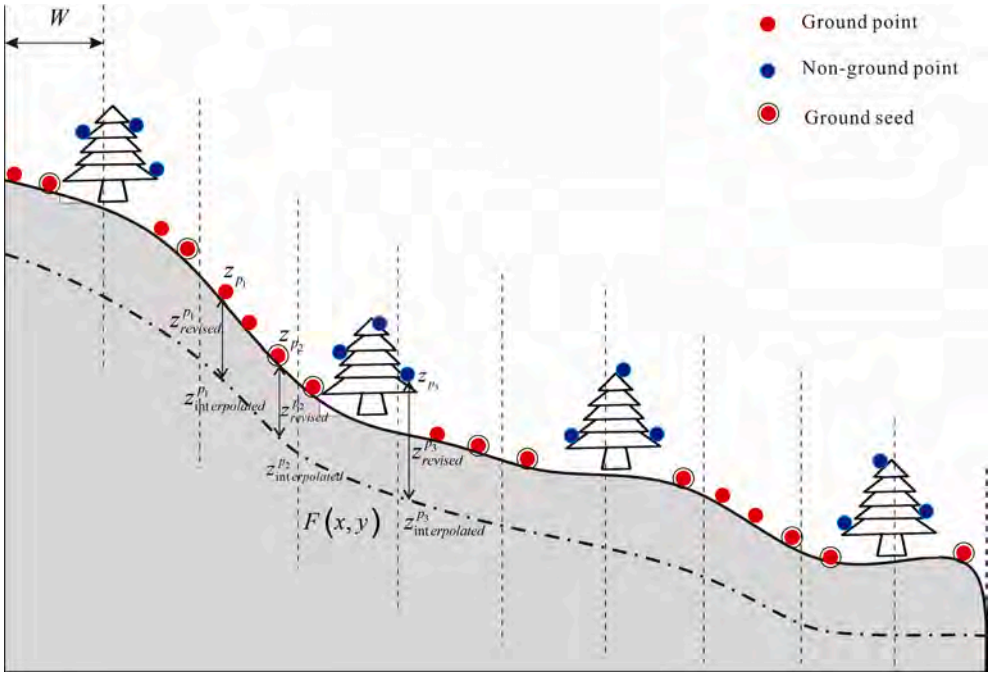

Fig. 4. The sketch map of highly rugged terrain and the generated trend surface. The red points represent ground points, while the blue points indicate non-ground points. The red points with excircles are the lowest ground seeds within the filtering window W. z^{p_i} is the original elevation; $z^{p_i}_{revised}$ is the revised elevation; $z^{p_i}_{interpolated}$ is the interpolated elevation. $F(x,y)$ represents the trending surface generated using RBF interpolator with ground seeds. (For interpretation of the references to colour in this figure legend, the reader is referred to the web version of this article.)

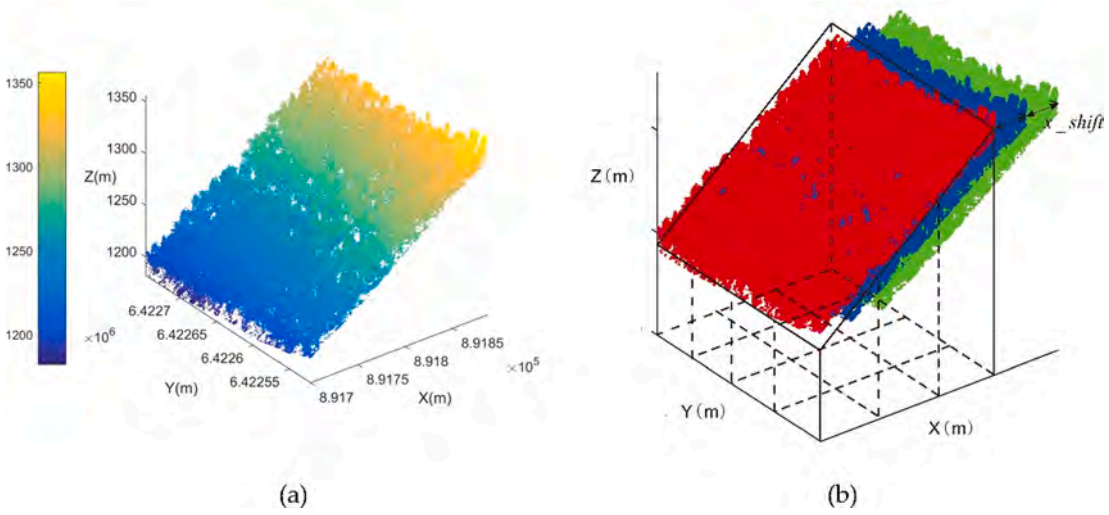

Fig. 5. The sketch map of ground seeds acquisition. (a) Point clouds colored by elevations. (b) The shifted point clouds in x direction. The red points are the original points, while the blue and green points are the shifted points in x direction with *shift* and $2*shift$, respectively. (For interpretation of the references to colour in this figure legend, the reader is referred to the web version of this article.)

earth primitives and should not calculate their horizontal bounding boxes.

As shown in Fig. 3 (a), each object primitive is first partitioned into grids at horizontal direction. The grid side is set to be 1 m in this paper. The horizontal bounding box can be calculated according to x and y coordinates of the points as shown in Fig. 3 (b). This procedure can be written as Eqs. (5) and (6).

$$M = floor\left(\frac{max\left(Obj^i.x\right) - min\left(Obj^i.x\right)}{cellsize}\right) + 1 \tag{5}$$

$$N = floor\left(\frac{max\left(Obj^i.y\right) - min\left(Obj^i.y\right)}{cellsize}\right) + 1 \tag{6}$$

where $M \times N$ is the size of the horizontal bounding box, $Obj^i.x$ and $Obj^i.y$ are x and y coordinates of each point in the i-th object primitive. *cellsize* is the size of the grid, $floor(\Delta)$ indicates round down.

2.3. Point cloud detrending

Most morphological filtering methods cannot work well in the highly rugged terrains with steep slopes. This is because most points on the steep terrains own abrupt elevations. The results of these points after morphological top-hat transformation are generally larger than the filtering threshold. Thus, these abrupt terrain points are easily misclassified as objects. Fig. 4 shows that the elevation of point p_1 is obvious much higher than that of point p_2. Ground point p_1 will be filtered when using morphological operations. That's why most morphology-based filtering methods conclude that morphological filters cannot protect terrain details well.

To solve this problem, this paper conduct point cloud detrending with the help of a trending surface generated using ground seeds. As mentioned above, the filtering window size can be determined according to the mean shift segmentation results. This paper selects the lowest points within the filtering windows W as ground seeds. As shown in Fig. 4, the red points with excircles are the ground seeds. Then a trending surface is generated based on these ground seeds using a radial basis function (RBF) interpolator. The trending surface is defined as Eq. (7).

$$F(x,y) = \sum_{i=1}^{n} \lambda_i \phi(\|p - p_i\|) - \delta h \tag{7}$$

where λ_i is the coefficient, $\phi(\cdot)$ is a Gaussian basis function, and $\|p - p_i\|$ represents the distance between points p and p_i. In this paper, a constant height shift δh is added to make the built trending surface always lower than the observed surface. δh used here is to avoid the influence of interpolation fitting error when building the trending surface. As shown in Fig. 4, the ground seeds are generally sparse. When generating the trending surface based on these sparse ground seeds it is easy to cause fitting errors. As a result, some parts of the trending surface may be higher than the observed surface. Obviously, it is unreasonable. By subtracting the trending surface with a constant, it will be ensured that the trending surface is always lower than the observed surface. In practice, δh is set to 3 m.

When the trending surface is generated, point cloud detrending can be realized by subtracting the elevation values of each point on the trending surface from their corresponding observed elevations. As shown in Fig. 4, $z^{p_1}_{revised}$, $z^{p_2}_{revised}$ and $z^{p_3}_{revised}$ are the revised elevations of points p_1, p_2 and p_3. The revised elevations are obtained by subtracting the interpolated elevations ($z^p_{interpolated}$) from their observed elevations (z_p). That is, $z^p_{revised} = z_p - z^p_{interpolated}$. Clearly, $z^p_{interpolated}$ can be calculated according to Eq. (7). In other words, $z^p_{interpolated}$ is equal to $F\left(x_p, y_p\right)$. As shown in Fig. 4, although z_{p_1} is much higher than z_{p_2}, $z^{p_1}_{revised}$ is close to $z^{p_2}_{revised}$ after point cloud detrending. It is because that $z^{p_1}_{interpolated}$ is also much high than $z^{p_2}_{interpolated}$as shown in Fig. 4. As a result, the revised elevations of these two points are close after the observed elevations (z_p) minus the interpolated elevations ($z^p_{interpolated}$). Moreover, although non-ground point p_3 is lower than ground point p_2, after transformation $z^{p_3}_{revised}$ is larger than $z^{p_2}_{revised}$. In so doing, we can try to make sure that object points are always higher than ground points, thereby reducing filtering omission errors in abrupt terrains.

As shown in Fig. 4, the key for point clouds detrending is generating the trending surface. To build a precise trending surface, the ground seeds should be accurate and enough. From Fig. 4, it can be found that the ground seeds can be easily acquired by locating the lowest points within the filtering windows. However, the acquired ground seeds will be less if the window size is larger. Fewer ground seeds cannot generate an accurate trending surface especially when encountering sloped terrains.

Fig. 5 (a) shows a sloped terrain which is covered by dense forests. To obtain ground seeds, the points should be projected onto the $x - y$ plane, which is partitioned into grids under the current filtering window.

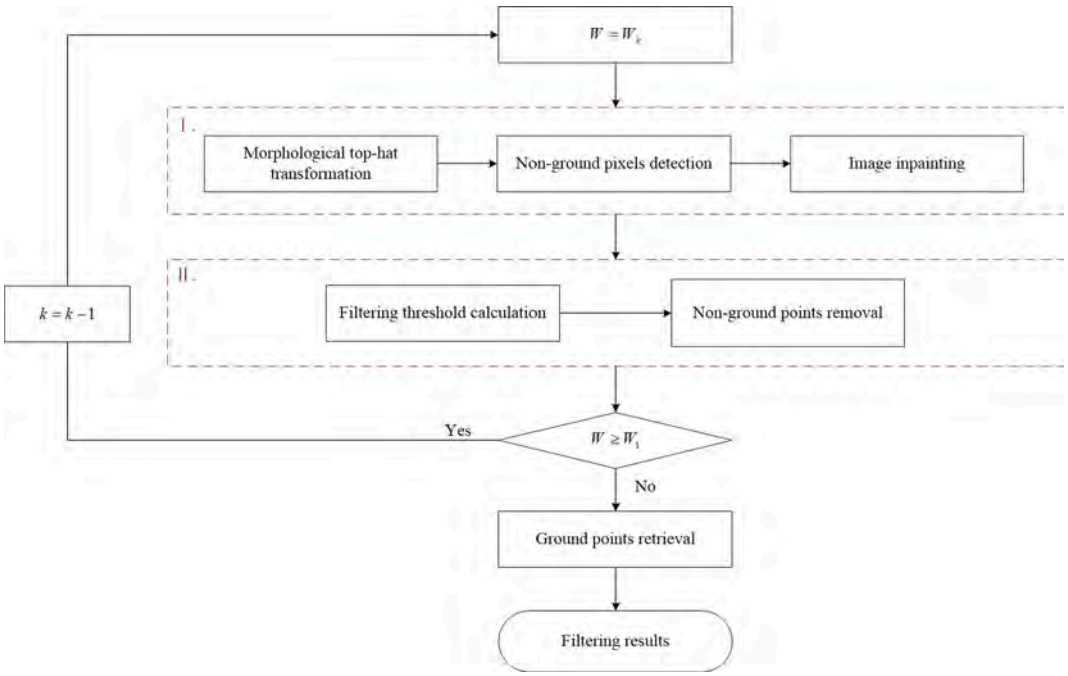

Fig. 6. Flowchart of the proposed morphological filtering method.

Obviously, larger window size results in less ground seeds. To acquire more ground seeds, this paper tries to shift the point clouds in x and y directions. As we know, the ground seeds are the points fallen into the grids with the lowest elevations. Thus, the grids can only capture limited lowest points within fixed local areas. However, if we shift the point clouds gradually, the local areas corresponding to each grid will be changed. That is to say the lowest points within the grids will be changed. Thus, more ground seeds can be captured by the grids.

In Fig. 5 (b), the red points are the original points, while the blue and green points are the shifted points in x direction with *shift* and $2*shift$, respectively. In each shifted process, only the points fallen into the scope of the original points are used to locate the ground seeds. This procedure can be written as Eq. (8).

$$shifted\_pts = \left\{ P(x_i + x\_shift, y_i + y\_shift, z_i) \middle| \begin{array}{l} min(x) \leqslant x_i + x\_shift \leqslant max(x); x\_shift \in [-2*shift, 2*shift], y\_shift = 0 \\ \cup \\ min(y) \leqslant y_i + y\_shift \leqslant max(y); y\_shift \in [-2*shift, 2*shift], x\_shift = 0 \end{array} \right\} \tag{8}$$

where $P(x, y, z)$ is the original point clouds. *x_shift* and *y_shift* are the shifted stepsizes in x and y directions. $min(x)$, $max(x)$, $min(y)$ and $max(y)$ indicate the scope of the original points. *shift* is the stepsize, which is defined as one fifth of the window size in this paper. Thus, the *x_shift* can be set as $[-2*shift, -shift, 0, shift, 2*shift]$respectively in each time. As a result, five times of ground seeds will be obtained. Of course, *shift* can be set to other values, such as one third of the window size. Consequently, three times of ground seeds can be acquired. Thus, the stepsize can be set empirically. It only affects the number of final obtained ground seeds. Note that when shifting the point clouds in x direction, *y_shift* should be equal to zero. Similarly, when shifting the point clouds in y direction, *x_shift* should be equal to zero.

2.4. Progressive morphological filtering

As mentioned above, object primitives $(Obj_1, Obj_2, \cdots, Obj_k)$ can be acquired by using mean shift segmentation method. In this paper, window sizes $(W_1, W_2, \cdots, W_k)$ are set as the horizontal sizes of object primitives. Note that window sizes are sorted in ascending order. In other words, W_{k-1} should be smaller than W_k. The benefits of setting window sizes as the horizontal sizes of object primitives are twofold. On the one hand, the maximum filtering window can be obtained automatically, which improves the automation and robustness of the filter for unknown environments. On the other hand, traditional morphological filtering methods always roughly set window sizes exponentially increasing. This setting is non-principled. In this paper, all the filtering windows are set according to the sizes of object primitives, which can reduce iteration times. Meanwhile, the filtering efficiency can be improved.

Fig. 6 is the flowchart of the proposed morphological filtering approach. The proposed morphological filter is processed in an iterative manner with filtering windows downsizing. The iteration is started with the largest window size W_k, which corresponds to the largest size of object primitives. Thereafter, morphological top-hat operation is applied to detect non-ground pixels.

In morphological top-hat transformation, three operations are involved, including erosion, dilation and opening. These morphological operations are defined as Eqs. (9)–(12).

$$E_W[DSM(x,y)] = min\{DSM(x+i, y+j) | i,j \in W \& (x+i, y+j) \in DSM\} \tag{9}$$

$$D_W[DSM(x,y)] = max\{DSM(x+i, y+j) | i,j \in W \& (x+i, y+j) \in DSM\} \tag{10}$$

$$O_W[DSM(x,y)] = D_W[E_W[DSM(x,y)]] \tag{11}$$

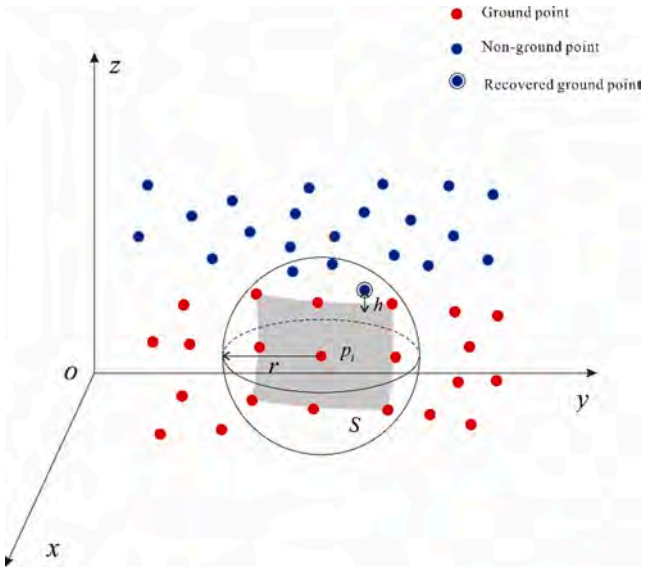

Fig. 7. The sketch map of ground points retrieval. Red points are ground points, while blue points are non-ground points. The blue point with an excircle is a recovered ground point. r is the radius for locating point p_i's neighbors. S is the constructed surface using these neighbors. h is the residual from the point to the surface S. (For interpretation of the references to colour in this figure legend, the reader is referred to the web version of this article.)

$$TH_W[DSM(x,y)] = DSM(x,y) - O_W[DSM(x,y)] \tag{12}$$

where $E_W[\cdot]$ is the morphological erosion, in which the minimum pixel value within the filtering window W is achieved. The pixel value mentioned here is equivalent to the value of each grid in $DSM(x,y)$, which can be obtained by seeking the lowest elevation of points fallen into the grid. $D_W[\cdot]$ is the morphological dilation, where maximum pixel value within the filtering window W is achieved. $O_W[\cdot]$ is the morphological opening, which is realized using morphological erosion followed by morphological dilation. $TH_W[\cdot]$ is the morphological top-hat transformation, which is realized by subtracting the morphological filtering result from the original data. Non-ground pixels can be detected if the morphological top-hat transformation results are larger than the filtering threshold, which can be calculated automatically according to the filtering window size as recommended by Zhang et al. (2003) [19].

When non-ground pixels are detected and removed, this paper fills these pixels using an image inpainting technique as recommended by Pingel et al. (2013) [24] and Özcan and Ünsalan (2017) [40]. The image inpainting technique tries to fill blank pixels using the nearest neighboring pixels. Using this technique, the digital terrain model (DTM) can be obtained in each iteration. Moreover, from Fig. 6, it can be found that the non-ground pixels are detected and removed iteratively. Thus, the obtained DTM will be changed from rough to accurate. To remove non-ground points, this paper calculates the residuals between the points and DTM. If the residuals are larger than the threshold, the points are labeled as non-ground points and removed. The threshold is calculated as the squared power of the slope of the obtained DTM [40]. In so doing, points on the abrupt terrains can be protected from removal since the slopes of these places are larger and the corresponding filtering thresholds will be larger. The residual $z^i_{residual}$ and threshold tre are calculated as Eqs. (13) and (14).

$$z^i_{residual} = z_i - z^i_{DTM} \tag{13}$$

$$tre = \rho + \Delta^2 \tag{14}$$

where z_i is the observed elevation of each point, z^i_{DTM} is its corresponding elevation on the DTM. Δ is the local slope of the DTM. ρ is a constant, which is set to 0.3 m in this paper. It means that the points with the elevation residuals smaller than 0.3 m will be accepted as ground points when the local slope of the DTM is equal to zero. In general, ρ plays a role of a compromise between the omission error and the commission error. A larger ρ means that more low points including some low shrubs will be accepted as ground points. Thus, the commission error may be larger. As a contrast, smaller ρ will lead to larger omission error. It is because some points on the abrupt terrains will be rejected as non-ground points. Generally speaking, ρ is determined experimentally [40].

Considering that the progressive morphological filter does not utilize the geometric characteristics to classify ground points from object points [47]. Some ground points on the protruding terrains are easily wrongly classified as object points and filtered. As a result, the terrain details cannot be protected effectively. To solve this problem, this paper recovers some filtered ground points by adopting the surface-based filtering strategy.

As shown in Fig. 7, the red and blue points are ground and non-ground points obtained using the progressive morphological filter. This paper tries to recover some non-ground points that are close to terrains as ground points. The retrieval procedure is carried out as follows:

i. Traverse each point p_i in the ground points set $\{Gpts\}$ and find its closest ground neighbors within r radius that is equal to the grid size used in Eq. (5).
ii. Construct a surface S using these ground neighbors by means of the RBF interpolator.
iii. Locate the nearest non-ground neighbors from non-ground points set $\{NGpts\}$ within r radius surrounding point p_i.
iv. Calculate the residuals h from these non-ground neighbors to the constructed surface S. If h is less than the threshold δz, the corresponding non-ground point will be recovered as a ground point.

Steps i-iv are repeated until all the ground points in $\{Gpts\}$ are traversed. All the recovered ground points will be added in $\{Gpts\}$.

Table 1
Acquisition parameters for the ALS benchmark [55].

Study area	Country	Plots	Size (ha)	Point density (pts/m^2)	Sensors
Saint-Agnan	France	1	1.0	13	Riegl LMS-Q560
Cotolivier	Italy	3	0.4	11	Optech ALTM 3100
Berner Jura	Switzerland	1	0.1	5	Leica ALS 70
Montafon	Austria	1	0.3	22	Riegl LMS-Q560
Pellizzano	Italy	2	0.3	95–121	Riegl LMS-Q680i
Asiago	Italy	3	0.4	11	Optech ALTM 3100
Tyrol	Austria	3	1.2	4–10	Optech ALTM 3100
Leskova	Slovenia	4	0.8	30	Riegl LMS-Q560

3. Results and validation

This paper adopts abundant datasets located in different forest environments for testing the performance of the proposed method. These datasets are provided by a research project named NEWFOR (NEW technologies for a better mountain FORest timber mobilization) [54]. The benchmark locates in total eight study areas in five different countries, which covers various terrain environments and forest types [55]. These airborne laser scanning (ALS) datasets are acquired using different sensors and settings as tabulated in Table 1. There are 18 plots

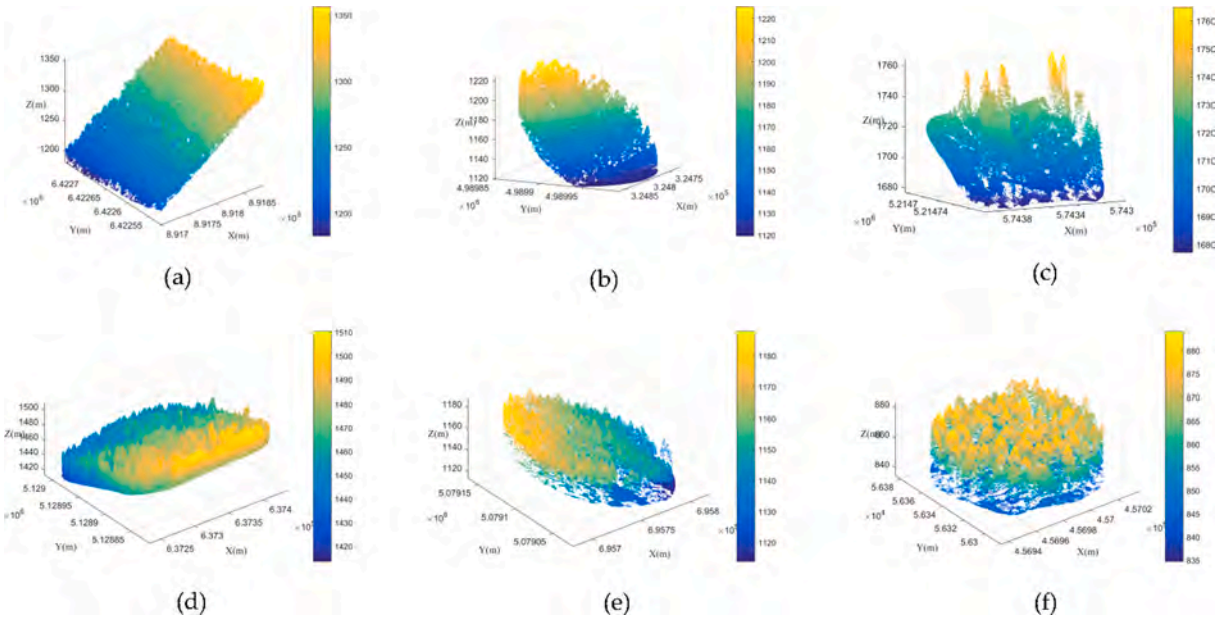

Fig. 8. 3-D point clouds in different plots: (a) Sample 01; (b) Sample 02; (c) Sample 06; (d) Sample 08; (e) Sample 09; (f) Sample 18. The point clouds are colored by elevations.

Table 2
Confusion matrix of the filtering results.

		Filtering results		
		Ground	Non-ground	
Reference	Ground	a	b	$e = a + b$
	Non-ground	c	d	$f = c + d$
		$g = a + c$	$h = b + d$	$n = a + b + c + d$

Table 3
Filtering accuracy of the proposed method towards 14 samples. (Due to the data property rights, four samples (05, 12, 13 and 14) are not provided by the project NEWFOR).

Samples	Type I error (%)	Type II error (%)	Total error (%)	Kappa (%)	RMSE (m)
01	2.28	0.38	0.62	97.20	0.65
02	2.96	1.57	1.88	94.63	0.56
03	1.07	1.07	1.07	97.47	0.36
04	0.48	0.08	0.23	99.51	0.30
06	1.41	2.02	1.70	96.58	1.08
07	1.00	2.05	1.84	94.28	0.36
08	1.71	0.13	0.32	98.47	0.29
09	1.19	0.01	0.26	99.21	0.55
10	2.80	1.26	1.55	94.98	0.59
11	3.75	0.25	0.56	96.49	1.13
15	9.43	0.69	2.28	92.16	0.54
16	9.96	0.68	2.64	91.85	0.69
17	2.06	0.03	0.29	98.68	0.47
18	1.49	0.17	0.35	98.47	1.28

with total sizes varying from 0.1 ha to 1.2 ha. The point densities of these plots vary from 5 points/m^2 up to 121 points/m^2. Thus, the experimental results of these datasets can indicate how about the filtering performance towards different point densities. The research project NEWFOR is initially introduced for improving forest timber evaluation and mobilization using ALS. In this paper, we use the benchmark to evaluate the performance of this method in different forested environments. Note that due to the data property rights, four datasets are not publicly available. Thus, 14 datasets are used for the experiments in this study.

Fig. 8 shows 3-D point clouds of six different plots in this benchmark. These figures shows that these samples cover different terrain environments with different point densities. Moreover, these datasets consist of different vegetation types. Thus, this benchmark will be helpful for testing the filtering performance in different forested environments. The NEWFOR project provides referenced digital terrain models (DTMs) with 1×1 or 0.5×0.5 spatial resolution. Therefore, it will be easy to compare the filtered DTM with the referenced DTM. The difference between the filtered and the referenced DTM is accessed using root mean square error (RMSE). It is defined as Eq. (15).

$$RMSE = \sqrt{\frac{\sum_{i=1}^{m}\sum_{j=1}^{n}\left(refer\_DTM(i,j) - DTM(i,j)\right)^2}{m \times n}} \tag{15}$$

where *refer_DTM* is the referenced DTM, while *DTM* is the filtered DTM. $m \times n$ is the total number of grids in the DTM.

To further analysis of the proposed method, four accuracy indexes including type I error ($T.I$), type II error ($T.II$), total error ($T.E$) and kappa coefficient (K) are calculated in this paper. Since NEWFOR does not provide the referenced ground and non-ground points in these 14 samples, this paper extracts the ground truth manually using a visualization analysis software called as CloudCompare [56]. These four indexes can be calculated according to the confusion matrix (Table 2) using Eqs. (16)–(19). The filtering results of the proposed method towards these 14 samples are shown in Table 3.

$$T.I = \frac{b}{e} \times 100\% \tag{16}$$

$$T.II = \frac{c}{f} \times 100\% \tag{17}$$

$$T.E = \frac{b+c}{n} \times 100\% \tag{18}$$

$$\begin{cases} P_0 = (a+d)/n \\ P_e = e/n \times g/n + f/n \times h/n \\ K = \dfrac{P_0 - P_e}{1 - P_e} \times 100\backslash\% \end{cases} \tag{19}$$

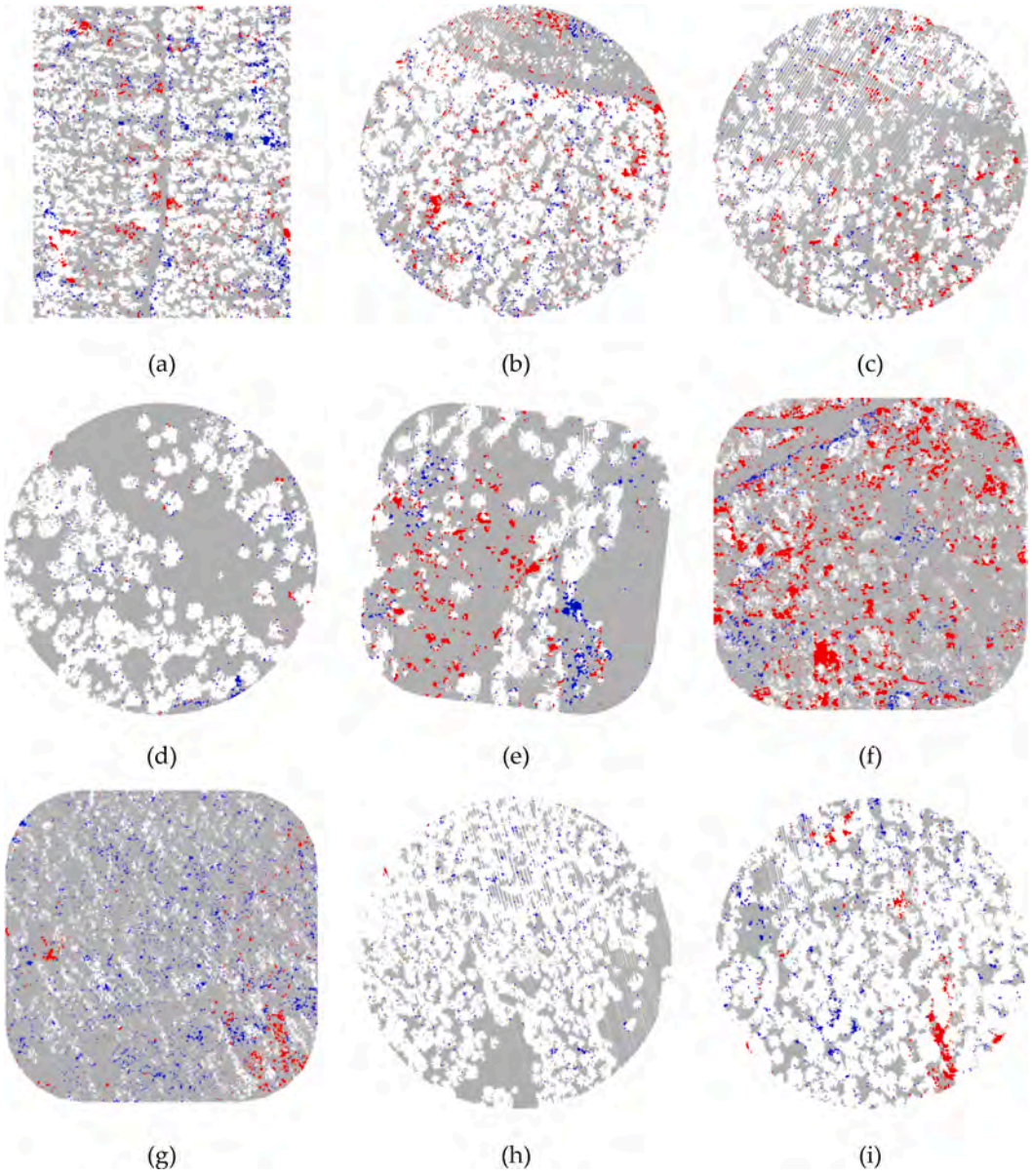

Fig. 9. Error distributions of the 14 samples: (a) Sample 01; (b) Sample 02; (c) Sample 03; (d) Sample 04; (e) Sample 06; (f) Sample 07; (g) Sample 08; (h) Sample 09; (i) Sample 10; (j) Sample 11; (k) Sample 15; (l) Sample 16; (m) Sample 17; (n) Sample 18. Grey points are the correctly classified grounds, blue points are the wrongly missed ground points and red points are the wrongly accepted non-ground points. (For interpretation of the references to colour in this figure legend, the reader is referred to the web version of this article.)

Table 3 shows that very good performance for all these 14 samples is achieved by the proposed filter. The largest total error is 2.64% (Sample 16), while all the kappa coefficients are larger than 90%. Moreover, only three samples' (Sample 06, Sample 11 and Sample 18) RMSEs are larger than 1.00. This indicates the obtained filtering results are very close to the referenced ground truth. Meanwhile, the difference between the filtered DTM and the referenced DTM is also very smaller. Fig. 8 shows the error distributions for the 14 samples. Grey points are the correctly classified ground points. As shown in Fig. 9 (a)-(n), most ground points are classified correctly. Blue points are the wrongly missed ground points, which lead to type I error (also called as omission error). Fig. 9 (k) and (l) show Samples 15 and 16 obtain larger type I errors, which can also be found from Table 3. Samples 15 and 16 obtain 9.43% and 9.96% type I errors, respectively. Both of these two errors are much larger than the ones of other 12 samples. Red points are the wrongly accepted non-ground points, which lead to type II error (also called as commission error). From Fig. 9 (f), it can be found that the type II error of Sample 07 is a little larger, which agrees with the findings of Table 3. Sample 07 achieves the largest type II error among all these 14 samples. In addition to Samples 06, 07, 15 and 16 causing larger filtering errors, all the other samples achieve very good filtering accuracy.

4. Discussion and comparison analysis

In this paper, five parameters are involved, namely h, δh, $shift$, ρ, and δz as tabulated in Table 4. To make the proposed method easy to implement, all the five parameters are set as fixed values. h is the bandwidth, which is related to the mean shift segmentation results. As mentioned in Section 2.1, the bandwidth h is the only parameter involved in the mean shift method. Since h determines the neighboring size of calculating mean shift vector ($Ms(v_i)$ in Eq. (1)), the value of h will influence the segmentation results. As recommended by Chen et al.

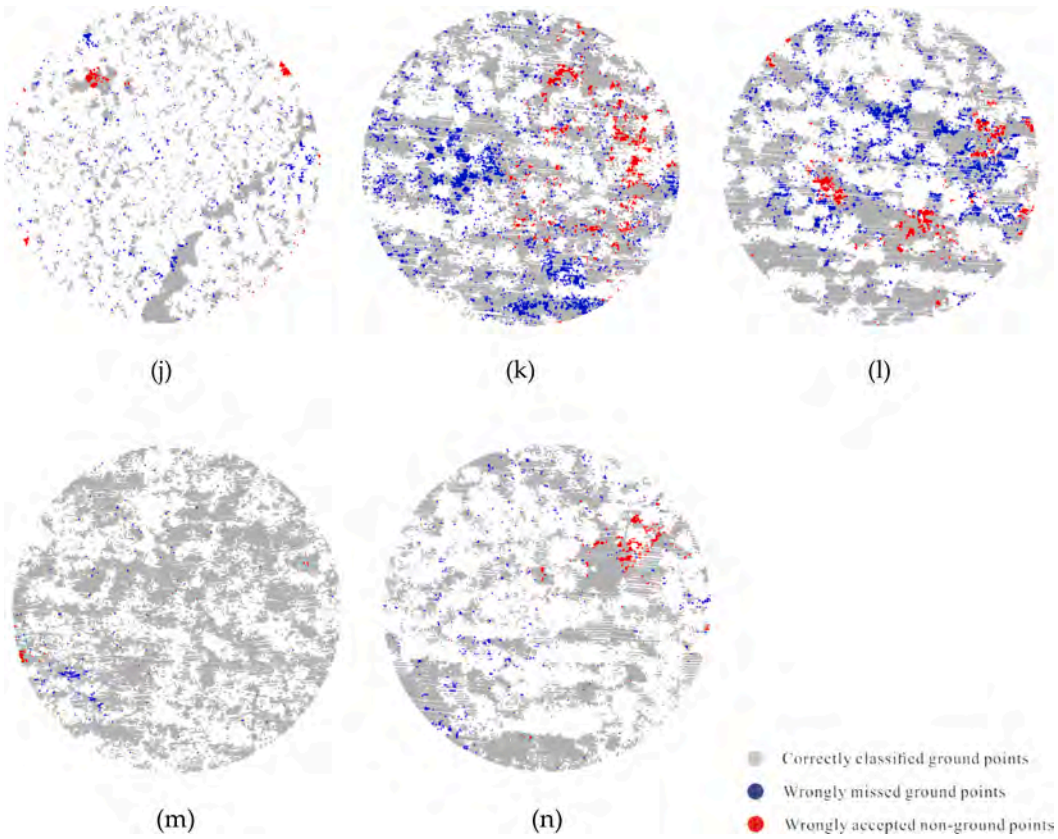

Fig. 9. (*continued*).

Table 4
Involved parameters and corresponding values used in this paper.

Parameters	Values
h	5 m
δh	3 m
shift	*windowsize*/5
ρ	0.3 m
δz	0.3 m

(2018), the bandwidth should be set according to the tree crown sizes in the forest environments. In this study, the mean shift method is used to segment object primitive for calculating the filtering window sizes. Individual tree does not need to be segmented very correctly. Thus, the bandwidth can be set as a constant roughly only if its value is a little larger than the crown sizes in the testing area. In this paper, the bandwidth is set to 5 m. δh is a parameter involved in Eq. (7). Eq. (7) is used to build a trending surface for calculating the interpolated elevation of each point. As shown in Fig. 4, the trending surface is generated based on the ground seeds using the RBF interpolator. In general, the interpolating process is easy to cause interpolation fitting error. As a result, some interpolated elevations may be higher than the actual observed elevations. Obviously, it is unreasonable. To avoid this, a height shift δh is added to the trending surface. δh can be set to any constant only if its value is larger than the interpolation fitting error. In this paper, δh is set to 3 m. *shift* is a parameter used for obtaining more ground seeds. It represents a stepsize when shifting the point clouds in $\times$ or y direction. In this paper, the stepsize is set to one fifth of the window size. It means that the point clouds will be shifted -2**shift*, $-$**shift*, 0, *shift*, and 2**shift* respectively in each time. As a result, five times of ground seeds will be obtained. Of course, *shift* can be set to other values, such as one third of the window size. Consequently, three times of ground seeds can be acquired. Thus, the stepsize can be set empirically. It only affects the number of final obtained ground seeds. ρ is a constant parameter mentioned in Eq. (14). Eq. (14) is used for calculating the filtering threshold automatically. In Eq. (14), ρ represents a fixed height value. It means the points with the residuals smaller than ρ will be accepted as ground points when the local slope of the DTM is equal to zero. As mentioned in Section 2.4, ρ plays a compromise between the omission and commission errors. There is no best setting for it. In general, ρ is set experimentally. In this paper, ρ is set to 0.3 m. δz is the threshold used for recovering the filtered ground points. It is mentioned in the fourth step of the ground points retrieval procedure. For most morphological filtering methods, they are easy to flatten terrain details. In other words, the points on the abrupt terrains are easy to be filtered as non-ground points. To recover these filtered ground points, this paper proposed a retrieval procedure. δz is the parameter that determines which point should be recovered. Similar to ρ, δz also affects the omission and commission errors of the filtering results. Larger δz means more points will be accepted as ground points. As a result, some low non-ground points may be wrongly classified as ground points. Thus, the commission error may be larger. Conversely, smaller δz will lead to less points to be recovered as ground points. It means that some ground points will be rejected as non-ground points. Consequently, omission error will be larger. Therefore, δz needs to be set experimentally. In this paper, δz is set to 0.3 m.

To compare the filtering performance objectively, four famous open-source filtering algorithms are also tested on these 14 samples. The first filtering algorithm designed by Kraus and Pfeifer (1998) is specially developed for wooded areas [41]. This method is one of the so-called surface-based filters, which is implemented in the FUSION v.3.8 software. The progressive morphological (PM) filter was proposed by Zhang et al. (2003). This filter removes non-ground points gradually using a series of filtering windows [19]. The PM algorithm is implemented in

Table 5
Type I error of the 14 samples of different filtering methods.

Samples	FUSION	PM	MCC	CSF	Proposed method
01	1.83	5.64	34.58	6.96	2.28
02	1.39	13.65	26.53	33.03	2.96
03	0.82	6.86	26.77	29.00	1.07
04	0.25	1.67	9.79	4.94	0.48
06	2.17	24.71	13.18	31.97	1.41
07	4.75	38.63	17.04	19.01	1.00
08	2.66	28.07	13.76	8.11	1.71
09	0.50	5.29	29.25	5.73	1.19
10	2.61	13.55	32.11	7.17	2.80
11	1.17	10.24	36.91	8.40	3.75
15	14.34	22.18	35.09	20.08	9.43
16	12.15	24.42	33.56	21.78	9.96
17	0.60	8.28	20.58	1.56	2.06
18	1.72	24.96	24.99	5.64	1.49
Ave	3.35	16.30	25.30	14.53	2.97
Min	0.25	1.67	9.79	1.56	0.48
Max	14.34	38.63	36.91	33.03	9.96
Std	4.37	10.87	9.04	10.98	2.98

Table 6
Type II error of the 14 samples of different filtering methods.

Samples	FUSION	PM	MCC	CSF	Proposed method
01	1.58	0.76	0.07	0.19	0.38
02	3.47	3.37	0.23	0.18	1.57
03	2.08	1.91	0.10	0.08	1.07
04	1.08	0.23	0.01	0.03	0.08
06	0.72	0.93	0.19	0.11	2.02
07	0.45	0.37	0.16	0.27	2.05
08	0.01	0.01	0.00	0.00	0.13
09	1.55	0.02	0.02	0.00	0.01
10	3.29	0.89	0.61	0.90	1.26
11	7.96	0.19	0.08	0.14	0.25
15	0.42	0.32	0.01	0.02	0.69
16	0.87	0.47	0.08	0.08	0.68
17	0.18	0.02	0.03	0.01	0.03
18	0.60	0.07	0.02	0.01	0.17
Ave	1.73	0.68	0.12	0.14	0.74
Min	0.01	0.01	0.00	0.00	0.01
Max	7.96	3.37	0.61	0.90	2.05
Std	2.09	0.93	0.16	0.23	0.73

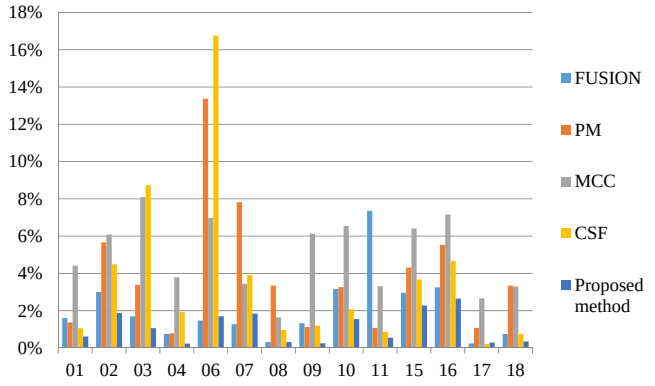

Fig. 10. Comparison of total errors of different filtering methods for the 14 samples.

ALSPAT v.1.0. MCC-LiDAR v.2.1 is developed for filtering in forested environments. Like FUSION v. 3.8 software, MCC is also a surface-based filter. In this method, non-ground points are filtered iteratively if their elevations exceed a threshold curvature that is calculated using a TPS built surface [42]. CSF is a famous filtering algorithm proposed recently, which is integrated in a 3-D point cloud and mesh processing software named CloudCompare [56]. CSF is also a surface-based filtering method,

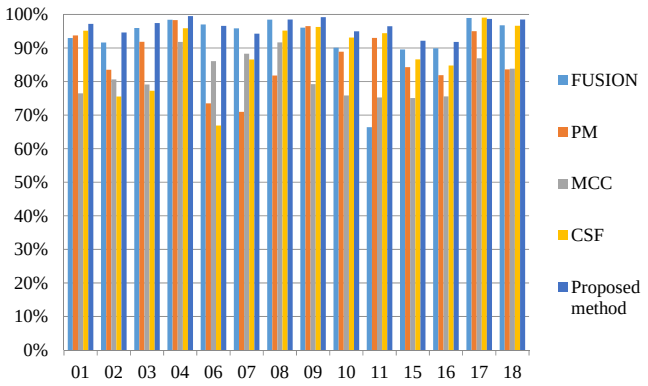

Fig. 11. Comparison of kappa coefficients of different filtering methods for the 14 samples.

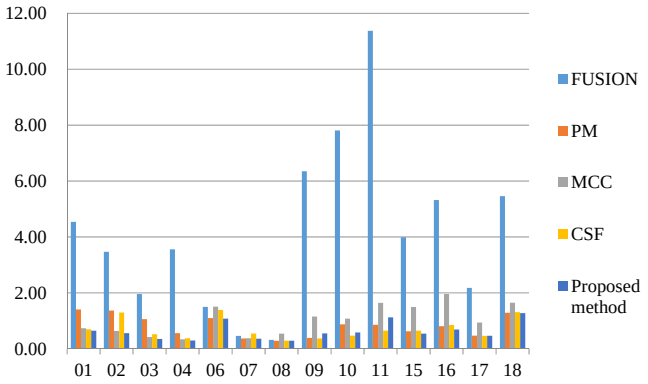

Fig. 12. Comparison of RMSEs of different filtering methods for the 14 samples.

which simulates the physical process of cloth-touching objects. The advantage of CSF is that the involved parameters are easy to be set.

The filtering results of these four famous filters and the proposed filter are shown in Tables 5 and 6 and Figs. 10–12. Tables 5 and 6 indicate the type I and II errors of the 14 samples of these five filtering methods. The average (Ave), Minimum (Min), Maximum (Max) and Standard deviation (Std) of the errors for the 14 samples are also calculated to test the robustness of the filters towards different forested environments. For type I error, this paper achieves the minimum average value (2.97%) comparing with that of other four methods. It means that the proposed filter can preserve terrain details much better the other filters. In addition to the FUSION method, the average of type I errors of PM, MCC and CSF are all larger than 10%. Moreover, the standard deviation of type I error of the proposed method is also smaller than that of other filtering methods. Therefore, we can conclude that the proposed filter owns strong filtering robustness towards different forested terrains. In terms of type II error, all the five filtering methods perform very well in all the 14 samples. The average of type II errors of four filters (PM, MCC, CSF and the proposed method) are all smaller than 1%. Meanwhile, the corresponding standard deviations of type II errors are also very smaller. The maximum type II error of this paper is 2.05%, which is much smaller than that of the FUSION method. Therefore, we can conclude that this method can eliminate the non-ground points effectively.

Figs. 10–12 show the comparison results of total errors, kappa coefficients and RMSEs of the five filtering methods. From Fig. 10, it can be found that only two samples' (Samples 15 and 16) total errors of the proposed method are larger than 2%. Among all the 14 samples, this paper achieves the smallest total errors for 11 samples, including Samples 01, 02, 03, 04, 08, 09, 10, 11, 15, 16 and 18. Consequently, this

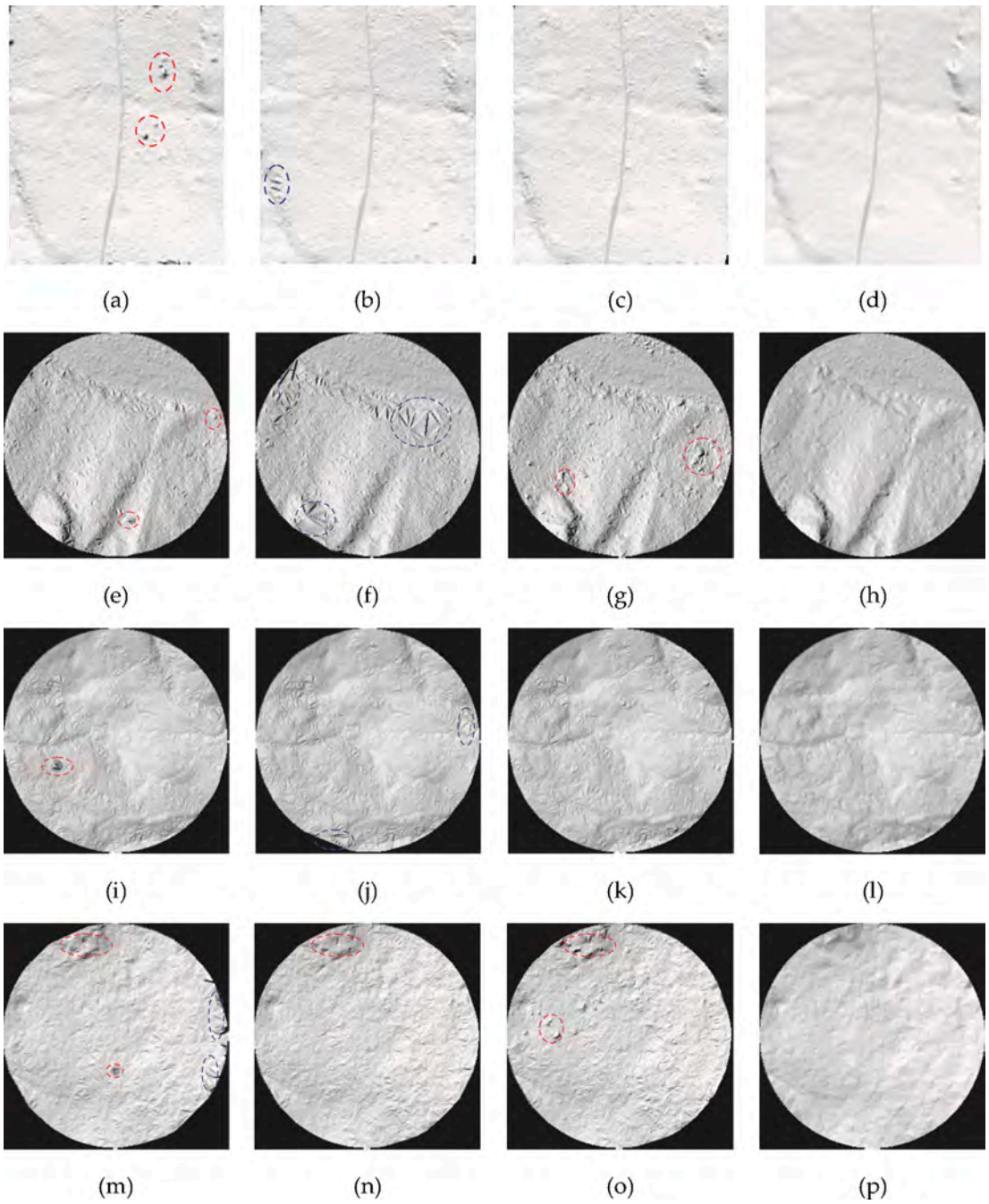

Fig. 13. Comparison of DTMs of different filtering methods towards different forested areas. (a)-(d) are the DTMs of Sample 01, (e)-(h) are the DTMs of Sample 02, (i)-(l) are the DTMs of Sample 04, and (m)-(p) are the DTMs of Sample 10. The first column indicates the DTMs of the MCC method. The second column indicates the DTMs of the CSF method. The third column indicates the DTMs of the proposed method. The fourth column indicates the referenced DTMs. The red dotted ellipse represents the commission error, while the blue dotted ellipse represents the omission error. (For interpretation of the references to colour in this figure legend, the reader is referred to the web version of this article.)

paper achieves 1.11% average total error, which is much smaller than that of other filtering methods. Fig. 11 indicates all the kappa coefficients of the 14 samples are larger than 90%. The average kappa coefficient of the proposed method is 96.43%, which is also the highest average kappa coefficient among these five filters. Fig. 12 indicates that the proposed filter achieves the smallest RMSE for 11 samples, including Samples 01, 02, 03, 04, 06, 07, 08, 10, 15, 16 and 18. The average RMSE of the proposed method is 0.63, which is the best filtering result for generating DTM.

Fig. 12 shows that MCC, CSF and the proposed filtering method can achieve very good RMSE results. To further analysis the proposed method, the generated DTMs of the proposed method with the ones of the MCC and CSF methods are compared. MCC is selected because previous studies have shown that this method can obtain the best overall performance towards forested environments [48]. CSF is a very famous filtering method in recent years. This method is easy to use and robust to different terrains. In addition to the DTMs generates using filtering results, this paper also shows the referenced DTMs provided by the project NEWFOR for the comparison analysis. The comparison results are shown in Fig. 13. Four samples with different forested environments are selected for the comparison. The first row shows the DTMs of Sample 01. The second row shows the DTMs of Sample 02. The third row shows the

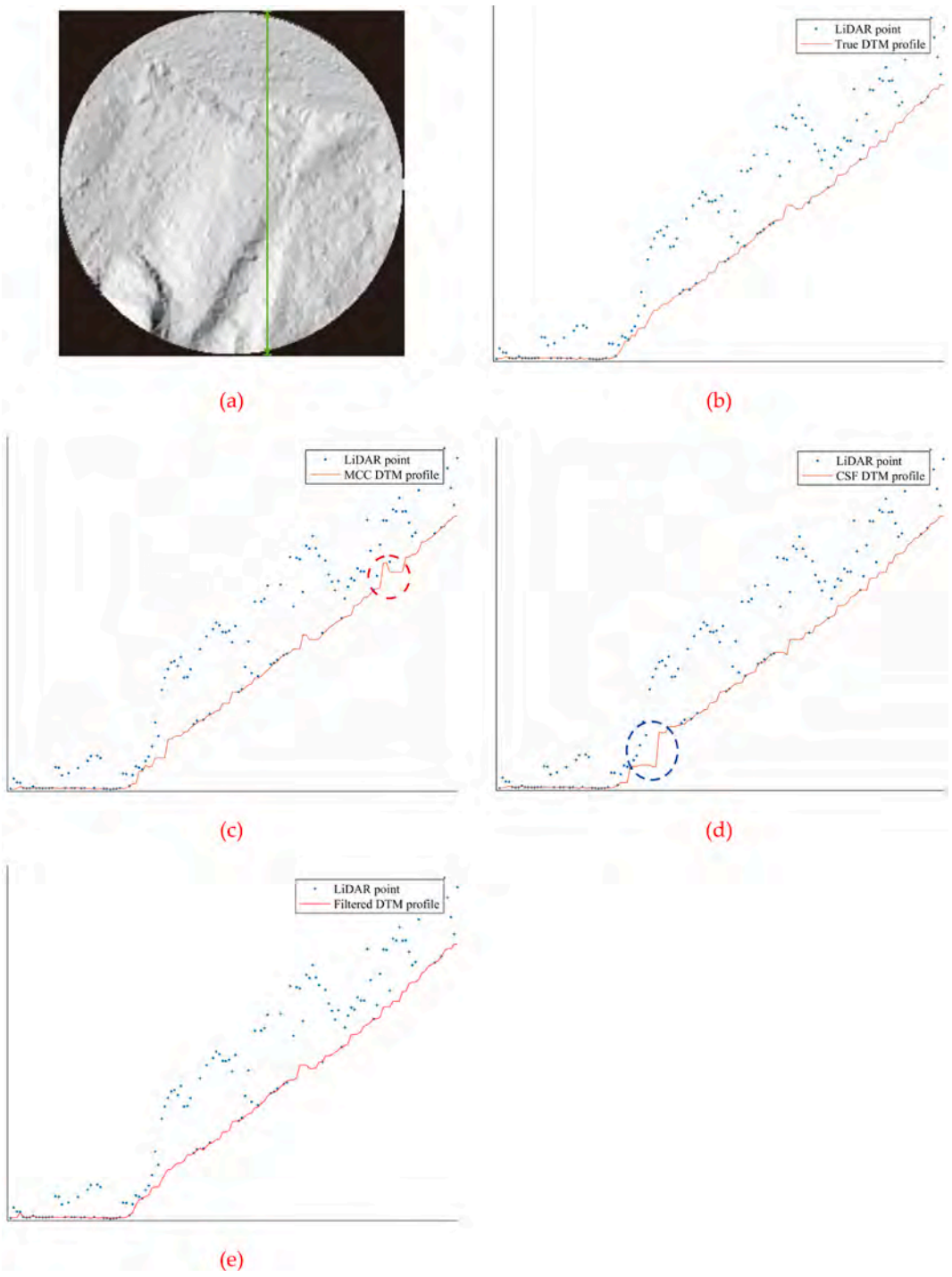

Fig. 14. Comparison of the cross-section profiles of the DTMs generated by different methods towards Sample 02. (a) the true DTM generated from the true ground points; (b) The cross-section profile (green line in (a)) of the true DTM; (c) the cross-section profile of the MCC filtered DTM; (d) the cross-section profile of the CSF filtered DTM; (e) the cross-section profile of the proposed filtered DTM. The red dotted ellipse represents the commission error, while the blue dotted ellipse represents the omission error. (For interpretation of the references to colour in this figure legend, the reader is referred to the web version of this article.)

DTMs of Sample 04. The fourth row shows the DTMs of Sample 10. In each row, DTMs of MCC, CSF, the proposed method and the reference are listed respectively. In Sample 01, MCC tends to produce artificial terrains due to accepting non-ground points as ground points as shown in Fig. 13 (a). From Fig. 13 (b), it can be found that CSF has difficulties in preserving terrain details. CSF is easy to flatten protruding terrains, which can also be found in Fig. 13 (f) and (j). The proposed method seems to produce a better DTM (Figure (c)) when comparing with the referenced DTM as shown in Fig. 13 (d). In Sample 02, both the DTMs of MCC and the proposed method (Fig. 13 (e) and (g)) are close to the referenced DTM (Fig. 13 (h)) except that some small commission errors are existed. The DTM produced by CSF has a little larger omission error as shown Fig. 13 (f). In Sample 04, all the DTMs of these three filters (Fig. 13 (i), (j) and (k)) are as accurate as the referenced one (Fig. 13 (l)). In terms of Sample 10, CSF and the proposed method produce more accurate DTMs (Fig. 13 (n) and (o)) comparing with the referenced DTM (Fig. 13 (p)). As shown Fig. 13 (m), there are a little larger omission and commission errors in the DTM produced by MCC. All in all, from all the

comparison results mentioned above, this paper can produce more accurate DTMs with smaller omission and commission errors. In other words, the method in this paper can not only remove object points accurately but also protect terrain details effectively.

To see the details of the error distribution and understand what cause the commission and omission errors, this paper compared the cross-section profiles of the DTMs generated by different methods towards Sample 02. As shown in Fig. 14 (a), the true DTM was generated using the reference ground points. The green line represents the location of the cross-section on the DTM. Fig. 14 (b) shows the true DTM cross-section profile and LiDAR points. Compared with the true DTM cross-section profile, it can be found that the MCC method is easy to produce artificial terrains due to accepting non-ground points as ground points as shown in Fig. 14 (c). That's why the commission error of the MCC method is larger. In Fig. 14 (d), it is easy to find that the CSF method cannot protect terrain details well. Obviously, the protruding terrains are flattened by the CSF method as the blue dotted ellipse labeled in Fig. 14 (d). Consequently, the omission error of the CSF method is larger. Compared with the MCC and CSF methods, the proposed method can produce the most accurate DTM cross-section profile. As shown in Fig. 14 (e), the proposed method can protect the terrain details well while removing object points accurately.

5. Conclusion

Filtering of airborne LiDAR point clouds in forested area is a challenging task. This paper proposed an improved morphological filter for the DTM extraction under forest canopy, which is the first time combing mean shift segmentation with morphological filter. The mean shift segmentation is used for obtaining the object primitives. In so doing, the filtering window sizes can be determined automatically. Thus, the robustness and automation of the proposed method are improved. Point cloud detrending is proposed by generating a trending surface using the RBF interpolator, thereby improving the adaptation to sloped terrains. To acquire more ground seeds for generating an accurate trending surface, a point cloud shifting in x and y directions technique is proposed. Finally, the filtered ground points by progressive morphological filter are recovered by adopting the surface-based filtering strategy. 14 forested samples provided by the project NEWFOR are adopted for testing. Experimental results show that the proposed method can achieve the average type I error of 2.97%, which is the smallest one when compared to other four famous open-source filtering methods, including FUSION, PM, MCC and CSF. In terms of total error, kappa coefficient and RMSE, the proposed method also performs the best. This paper also compares the DTMs of MCC, CSF and the proposed method with the referenced ones. The comparison results show that the proposed method can not only eliminate non-ground point accurately but also protect terrain details effectively.

Author contributions

Z.H. conceived the original idea of the study and drafted the manuscript. S.J. contributed to the revision of the manuscript. Y.X. and Y.N. performed the experiments. X.X. and N.L. made the experimental analysis.

Funding

This work was supported by the National Natural Science Foundation of China (NSF) (41801325, 41962018), the Natural Science Foundation of Jiangxi Province (20192BAB217010), the China Post-Doctoral Science Foundation (2019M661858), Education Department of Jiangxi Province (GJJ170449), Key Laboratory for Digital Land and Resources of Jiangxi Province, East China University of Technology (DLLJ201806), East China University of Technology Ph. D. Project (DHBK2017155) for their financial support.

Declaration of Competing Interest

The authors declare that they have no known competing financial interests or personal relationships that could have appeared to influence the work reported in this paper.

Acknowledgments

Authors would like to thank NEWFOR (NEW technologies for a better mountain FORest timber mobilization) for providing abundant datasets located in different forest environments.

References

[1] G. Vosselman, H.G. Maas, Airborne and terrestrial laser scanning, Whittles Publishing, Dunbeath, Scotland, 2010.
[2] B. Yang, R. Huang, Z. Dong, Y. Zang, J. Li, Two-step adaptive extraction method for ground points and breaklines from lidar point clouds, ISPRS-J. Photogramm. Remote Sens. 119 (2016) 373–389.
[3] L. Wallace, A. Lucieer, C. Watson, D. Turner, Development of a UAV-LiDAR system with application to forest inventory, Remote Sens. 4 (2012) 1519–1543.
[4] Z.Y. Hui, Y.J. Hu, S.G. Jin, Y.Z. Yevenyo, Road centerline extraction from airborne LiDAR point cloud based on hierarchical fusion and optimization, ISPRS-J. Photogramm. Remote Sens. 118 (2016) 22–36.
[5] Y. Li, B. Yong, P. Van Oosterom, M. Lemmens, H. Wu, L. Ren, M. Zheng, J. Zhou, Airborne LiDAR data filtering based on geodesic transformations of mathematical morphology, Remote Sens. 9 (2017) 1104.
[6] J. Hyyppä, H. Hyyppä, D. Leckie, F. Gougeon, X. Yu, M. Maltamo, Review of methods of small-footprint airborne laser scanning for extracting forest inventory data in boreal forests, Int. J. Remote Sens. 29 (2008) 1339–1366.
[7] Y. Wang, J. Pyörälä, X. Liang, M. Lehtomäki, A. Kukko, X. Yu, H. Kaartinen, J. Hyyppä, In situ biomass estimation at tree and plot levels: What did data record and what did algorithms derive from terrestrial and aerial point clouds in boreal forest, Remote Sens. Environ. 232 (2019), 111309.
[8] W. Xiao, S. Xu, S.O. Elberink, G. Vosselman, Individual tree crown modeling and change detection from airborne lidar data, IEEE J. Sel. Top. Appl. Earth Observations Remote Sensing 9 (8) (2016) 3467–3477.
[9] W. Zhang, P. Wan, T. Wang, S. Cai, Y. Chen, X. Jin, G. Yan, A novel approach for the detection of standing tree stems from plot-level terrestrial laser scanning data, Remote Sens. 11 (2019) 211.
[10] X. Zhu, A.K. Skidmore, R. Darvishzadeh, K.O. Niemann, J. Liu, Y.F. Shi, T.J. Wang, Foliar and woody materials discriminated using terrestrial LiDAR in a mixed natural forest, Int. J. Appl. Earth Obs. Geoinf. 64 (2018) 43–50.
[11] Z.Y. Hui, S.G. Jin, P.G. Cheng, Y.Y. Ziggah, L.Y. Wang, Y.Q. Wang, H.Y. Hu, Y. J. Hu, An active learning method for DEM extraction from airborne LiDAR point clouds, IEEE Access 7 (2019) 89366–89378.
[12] Z. Chen, B. Gao, B. Devereux, State-of-the-art: DTM generation using airborne LIDAR data, Sensors 17 (2017) 150.
[13] X. Meng, N. Currit, K. Zhao, Ground filtering algorithms for airborne LiDAR data: a review of critical issues, Remote Sens. 2 (2010) 833–860.
[14] X.Y. Liu, Airborne LiDAR for DEM generation: some critical issues, Prog. Phys. Geogr. 32 (2008) 31–49.
[15] G. Vosselman, Slope based filtering of laser altimetry data, IAPRS 33 (2000) 958–964.
[16] J. Susaki, Adaptive slope filtering of airborne LiDAR data in urban areas for digital terrain model (DTM) generation, Remote Sens. 4 (2012) 1804–1819.
[17] X.G. Lin, J.X. Zhang, Segmentation-based filtering of airborne LiDAR point clouds by progressive densification of terrain segments, Remote Sens. 6 (2014) 1294–1326.
[18] J. Kilian, N. Haala, M. Englich, Capture and evaluation of airborne laser scanner data, Int. Arch. Photogramm. Remote Sens. 31 (1996) 383–388.
[19] K.Q. Zhang, C. Shu-Ching, D. Whitman, S. Mei-Ling, Y. Jianhua, Z. Chengcui, A progressive morphological filter for removing nonground measurements from airborne LIDAR data, IEEE Trans. Geosci. Remote Sensing 41 (2003) 872–882.
[20] Q. Chen, P. Gong, D. Baldocchi, G. Xie, Filtering airborne laser scanning data with morphological methods, Photogramm. Eng. Remote Sens. 73 (2007) 175–185.
[21] Y. Li, H. Wu, H. Xu, R. An, J. Xu, Q. He, A gradient-constrained morphological filtering algorithm for airborne LiDAR, Opt. Laser Technol. 54 (2013) 288–296.
[22] Y. Li, B. Yong, H.Y. Wu, R. An, H.W. Xu, J. Xu, Q.S. He, Filtering airborne lidar data by modified white top-hat transform with directional edge constraints, Photogramm. Eng. Remote Sens. 80 (2014) 133–141.
[23] D. Mongus, N. Lukac, B. Zalik, Ground and building extraction from LiDAR data based on differential morphological profiles and locally fitted surfaces, ISPRS-J. Photogramm. Remote Sens. 93 (2014) 145–156.
[24] T.J. Pingel, K.C. Clarke, W.A. McBride, An improved simple morphological filter for the terrain classification of airborne LIDAR data, ISPRS-J. Photogramm. Remote Sens. 77 (2013) 21–30.
[25] Z.Y. Hui, L.Y. Wang, Y.Y. Ziggah, S.S. Cai, Y.P. Xia, Automatic morphological filtering algorithm for airborne lidar data in urban areas, Appl. Optics 58 (2019) 1164–1173.

[26] C. Chen, Y. Li, W. Li, H. Dai, A multiresolution hierarchical classification algorithm for filtering airborne LiDAR data, ISPRS-J. Photogramm. Remote Sens. 82 (2013) 1–9.
[27] P. Cheng, Z. Hui, Y. Xia, Y.Y. Ziggah, Y. Hu, J. Wu, An improved skewness balancing filtering algorithm based on thin plate spline interpolation, Appl. Sci. 9 (2019) 203.
[28] H. Hu, Y.L. Ding, Q. Zhu, B. Wu, H. Lin, Z.Q. Du, Y.T. Zhang, Y.S. Zhang, An adaptive surface filter for airborne laser scanning point clouds by means of regularization and bending energy, ISPRS-J. Photogramm. Remote Sens. 92 (2014) 98–111.
[29] D. Mongus, B. Žalik, Parameter-free ground filtering of LiDAR data for automatic DTM generation, ISPRS-J. Photogramm. Remote Sens. 67 (2012) 1–12.
[30] P. DEM Axelsson, generation from laser scanner data using adaptive TIN models, Photogramm. Eng. Remote Sens. 33 (2000).
[31] X. Meng, Y. Lin, L. Yan, X. Gao, Y. Yao, C. Wang, S. Luo, Airborne LiDAR point cloud filtering by a multilevel adaptive filter based on morphological reconstruction and thin plate spline interpolation, Electronics 8 (2019) 1153.
[32] J. Zhang, X. Lin, Filtering airborne LiDAR data by embedding smoothness-constrained segmentation in progressive TIN densification, ISPRS-J. Photogramm. Remote Sens. 81 (2013) 44–59.
[33] G. Sithole, G. Vosselman, Experimental comparison of filter algorithms for bare-Earth extraction from airborne laser scanning point clouds, ISPRS-J. Photogramm. Remote Sens. 59 (2004) 85–101.
[34] W. Zhang, J. Qi, P. Wan, H. Wang, D. Xie, X. Wang, G. Yan, An easy-to-use airborne LiDAR data filtering method based on cloth simulation, Remote Sens. 8 (2016) 501.
[35] S. Cai, W. Zhang, X. Liang, P. Wan, J. Qi, S. Yu, G. Yan, J. Shao, Filtering airborne LiDAR data through complementary cloth simulation and progressive TIN densification filters, Remote Sens. 11 (2019) 1037.
[36] D. Tóvári, N. Pfeifer, Segmentation based robust interpolation - A new approach to laser data filtering, Laser Scanning (2005) 12–14.
[37] C. Chen, Y. Li, C. Yan, H. Dai, G. Liu, J. Guo, An improved multi-resolution hierarchical classification method based on robust segmentation for filtering ALS point clouds, Int. J. Remote Sens. 37 (2016) 950–968.
[38] X. Hu, Y. Yuan, Deep-learning-based classification for DTM extraction from ALS point cloud, Remote Sens. 8 (2016) 730.
[39] H. Ni, X.G. Lin, J.X. Zhang, D. Chen, J. Peethambaran, Joint clusters and iterative graph cuts for ALS point cloud filtering, IEEE J. Sel. Top. Appl. Earth Observ. Remote Sens. 11 (2018) 990–1004.
[40] A.H. Ozcan, C. Unsalan, LiDAR data filtering and DTM generation using empirical mode decomposition, IEEE J. Sel. Top. Appl. Earth Observations Remote Sensing 10 (1) (2017) 360–371.
[41] K. Kraus, N. Pfeifer, Determination of terrain models in wooded areas with airborne laser scanner data, ISPRS-J. Photogramm. Remote Sens. 53 (1998) 193–203.
[42] J.S. Evans, A.T. Hudak, A multiscale curvature algorithm for classifying discrete return LiDAR in forested environments, IEEE Trans. Geosci. Remote Sensing 45 (2007) 1029–1038.
[43] C. Véga, S. Durrieu, J. Morel, T. Allouis, A sequential iterative dual-filter for Lidar terrain modeling optimized for complex forested environments, Comput. Geosci. 44 (2012) 31–41.
[44] A.S. Maguya, V. Junttila, T. Kauranne, Adaptive algorithm for large scale dtm interpolation from lidar data for forestry applications in steep forested terrain, ISPRS-J. Photogramm. Remote Sens. 85 (2013) 74–83.
[45] X. Zhao, Q. Guo, Y. Su, B. Xue, Improved progressive TIN densification filtering algorithm for airborne LiDAR data in forested areas, ISPRS-J. Photogramm. Remote Sens. 117 (2016) 79–91.
[46] L.i. Liu, S. Lim, A voxel-based multiscale morphological airborne lidar filtering algorithm for digital elevation models for forest regions, Measurement 123 (2018) 135–144.
[47] B. Bigdeli, H. Amini Amirkolaee, P. Pahlavani, DTM extraction under forest canopy using LiDAR data and a modified invasive weed optimization algorithm, Remote Sens. Environ. 216 (2018) 289–300.
[48] A. Luis Montealegre, M. Teresa Lamelas, J. de la Riva, A comparison of open-source LiDAR filtering algorithms in a mediterranean forest environment, IEEE J. Sel. Top. Appl. Earth Observ. Remote Sens. 8 (2015) 4072–4085.
[49] X. Zhao, Y. Su, W. Li, T. Hu, J. Liu, Q. Guo, A comparison of LiDAR filtering algorithms in vegetated mountain areas, Can. J. Remote Sens. 44 (2018) 287–298.
[50] C. Chen, M. Wang, B. Chang, Y. Li, Multi-level interpolation-based filter for airborne LiDAR point clouds in forested areas, IEEE Access 8 (2020) 41000–41012.
[51] A. Ferraz, F. Bretar, S. Jacquemoud, G. Gonçalves, L. Pereira, M. Tomé, P. Soares, 3-D mapping of a multi-layered mediterranean forest using ALS data, Remote Sens. Environ. 121 (2012) 210–223.
[52] W. Dai, B. Yang, Z. Dong, A. Shaker, A new method for 3-D individual tree extraction using multispectral airborne LiDAR point clouds, ISPRS-J. Photogramm. Remote Sens. 144 (2018) 400–411.
[53] W. Chen, X. Hu, W. Chen, Y. Hong, M. Yang, Airborne LiDAR Remote sensing for individual tree forest inventory using trunk detection-aided mean shift clustering techniques, Remote Sens. 10 (2018) 1078.
[54] NEWFOR Alpine Space Programme. European Territorial Cooperation. Available online: https://www.newfor.net/ (accessed on 4th March 2020).
[55] L. Eysn, M. Hollaus, E. Lindberg, F. Berger, J.-M. Monnet, M. Dalponte, M. Kobal, M. Pellegrini, E. Lingua, D. Mongus, et al., A benchmark of lidar-based single tree detection methods using heterogeneous forest data from the alpine space, Forests 6 (2015) 1721–1747.
[56] Girardeau-Montaut, D. Cloudcompare-open source project, Open-Source Project. Available online: http://www.cloudcompare.org/ (accessed on 4th March 2020).